



ASSESSMENT MATERIAL SELECTION FOR CHAIN - SUBMERGED SCRAPER CONVEYOR

GUNAWAN, AMIR ARIFIN, IRSYADI YANI, M.A. ADE SAPUTRA¹, BARLIN OEMAR,
ZULKARNAIN ALI LEMAN*, DENDY ADANTA¹, AKBAR TEGUH PRAKOSO¹

*Department of Mechanical Engineering, Faculty of Engineering, Universitas Sriwijaya, 30662
Indralaya, Sumatera*

**Corresponding author: zulkarnain@ft.unsri.ac.id*

(Received: 21 January 2023; Accepted: 16 February 2023; Published on-line: 1 March 2023)

ABSTRACT: Chain-submerged scrapper conveyor bottom ash handling in the petrochemical industry has failed several times and was repaired with AISI 420, which can only operate for three months. AISI 420 is recommended in applications requiring moderate corrosion resistance, high hardness, excellent wear resistance, and good edge retention in cutting surfaces. The initial cracks and fractures occur in the pin-link joint hole, which causes chain failure. Some evaluation has been performed for both as-received and failed links. It can be concluded that chain link failure occurs due to fatigue failure with low-stress levels. Microstructure observation, XRD, and hardness properties showed no significant difference in both as-received and failed links. Since the operating conditions of the chain are in a corrosive environment, experiencing dynamic loading and working temperatures between 23 °C and 60 °C, the selection of HSL materials such as AISI 4140 should be considered.

KEY WORDS: *chain submerged scrapper, failure, hardness, morphology, tensile*

1. INTRODUCTION

Submerged scraper conveyors are typically used to remove ash from power plant coal-fired boilers. Submerged Scraper Conveyors are made to extinguish, cool completely, and transport combustion residues like ash and slag without creating dust [1]. It successfully prevents the entry of outside air, which can impede combustion processes, while also preventing vapors and particulates from exiting. The Submerged scrapper conveyor, positioned under the bottom ash hopper, cools the hot bottom ash from the boiler furnace. The boiler receives water sealing from the submerged conveyor's water trough. The scrapper bar linked to the quality chain constantly moves slowly, draining the water from the ash as it does so. The wet ash is fed into a belt conveyor from the scraper conveyor and transported to a storage bin for later loading into trucks or wagons for final disposal or discharged into a sluice trench for transfer to a slurry sump.

Submerged scrapper conveyors have an operational temperature of 40-400°C with the operating environment of water with sulfate content of 25-32 ppm. There are several advantages to using a submerged scraper conveyor (SSC) in the industry. SSCs operate underwater, which greatly reduces the noise level compared to above-ground conveyors due to the material being conveyed underwater, and dust generation is significantly reduced. SSCs are highly efficient at moving large quantities of material. In terms of maintenance, the design of SSCs makes them relatively easy to maintain, as the chain and flight assembly can be easily accessed for repairs.

It is inevitable that ash residue will build up on the wall surface of a boiler furnace during the incomplete combustion of pulverized coal during the boiler's heating operation. As a result, the ash layers that accumulate could significantly reduce heat transfer to the steam cycle [2]. This necessitates a soot blowing operation for elimination of the resulting residues. Soot blowers are utilized in this operation, and high-pressure steam is aimed at a residue until it cracks from the impact [3, 4]. It is the mechanical and thermal strains created in the residue in this scenario that lead to its elimination [5]. The water from the SSC will cover the fallen slag once it has passed through the ash reject hopper [6]. Afterwards, the ash is sent to the bottom ash silo or ash pond through belt conveyors.

This study aims to assess material selection of submerged scrapper conveyors through metallurgy and mechanical analysis. Chain-submerged scrapper conveyor is made of the AISI 420, categorized as martensitic stainless steel.

2. BACKGROUND OF THE FAILURE

The submerged scrapper conveyor in the petrochemical industry was found to have failed when periodic inspections were carried out. Chain-submerged scrapper conveyor has failed several times and was repaired with material changes. The last material chain change with AISI 420 lasted only approximately three months. Medium-carbon AISI 420 martensitic stainless steel is recommended for use in applications requiring moderate corrosion resistance, high hardness, excellent wear resistance, and good edge retention in cutting surfaces. The microstructure and properties of this steel depend strongly on the hardening heat treatment, particularly the austenitizing treatment that the steel receives.

The fracture occurs in the pin-link joint hole in one or both end holes. The initial cracks were identified from the corrosion color, which was more concentrated than in other areas. There are two main areas where crack initiation occurs; first, in the area that experiences higher residual stresses due to changes in dimensions that are not streamlined (notch root); the second initial cracks occur in the middle of the pinhole. In both cases, in terms of loading condition, it is believed that the cracks occurred due to the influence of the interference fit pin-links joint assembly and cyclic loading. The failure of the chain-submerged scrapper conveyor can be seen in Fig. 1.



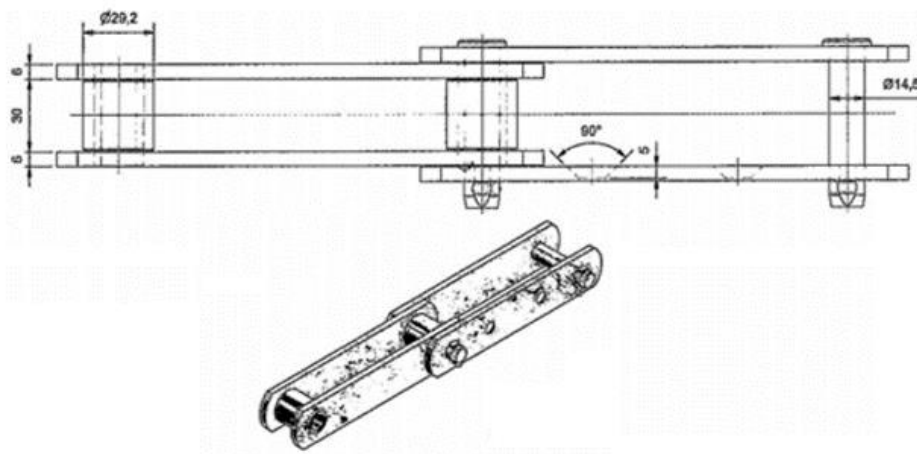


Fig. 1. Failure part of chain scrapper.

3. MATERIALS AND METHODS

One failed chain is used to test the composition of chain materials through the X-ray fluorescence (XRF) analysis method. X-ray fluorescence (XRF) is an analytical technique used to determine the elemental composition of a sample. It works by irradiating a sample with X-rays and measuring the energy spectrum of the emitted fluorescent radiation [7]. This process allows for precisely determining each element present in the sample and its concentration and distribution relative to other elements. The failed chain sections were subjected to visual examination and, subsequently, stereomicroscopic examination to understand the macro features of failure. Through this analysis, it will be possible to find the characteristics of fractures that apply to failed chains.

Chains that have failed are carried out with metallographic analysis to analyze phase changes. The analysis was carried out using standard metallographic procedures. Furthermore, mechanical properties analysis was carried out through tensile and hardness tests surrounding the hole to analyze distribution hardness. Phase changes that occur in the material chain will be investigated through X-Ray diffraction. X-rays are generated by a cathode ray tube, filtered to produce monochromatic radiation, collimated to concentrate, and directed toward the sample.

4. RESULTS AND DISCUSSION

To analyze correctly, it is necessary to know the elemental composition as well as to verify whether the material used is appropriate. The composition of the chain scrapper was analyzed using X-ray fluorescence (XRF) analysis. Table 1. shows that chrome and Mangan are the most prominent alloying element, with 12.18 and 0.42 wt%, respectively. Referring to the results of the XRF analysis can be sure that the failed chain is AISI 420. It is stainless steel with excellent hardenability and strength and great corrosion resistance properties.

Table 1: Chemical composition of failed chain

Elements	V	Cr	Mn	Fe	Zn	Mo
%	0.103	12.18	0.42	80.16	0.05	0.057

4.1. X-Ray Diffraction Analysis

X-Ray diffraction analysis is a typical means to determine the structure and relative configuration of solid compounds in an unequivocal way. X-Ray Diffraction (XRD) testing on Rigaku MiniFlex 600 with a Cu K α X-ray tube ($\lambda = 0.17889$ nm) in the Bragg–Brentano configuration. XRD result of chain material is shown in Fig. 2. XRD analysis shows there was not found another peak in the material sample.

The highest presents one peak (at 2θ angle of 44.9°) attributed to the martensite phase. The remaining peaks occurring at 37.2° , 39.3° , 40.3° , 42.5° , 43.3° , 45.6° , 48.8° , 51.5° , 55.7° and 57.7° correspond to the Fe_3C phase. The occurrence of the Cr_7C_3 and Cr_{23}C_6 phases could be suggested in the present case. Diffraction peaks occurred for 2θ angles of 37.2° , 39.3° , 43.3° , 48.8° , and 51.5° , but it should be noted that such peaks could also be indexed for the Fe_3C phase.

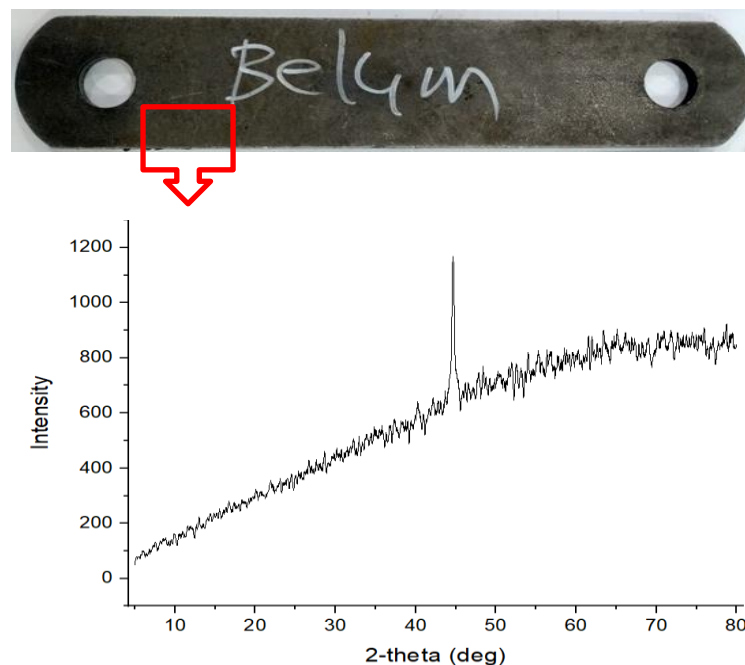


Fig. 2. XRD result of chain scrapper

4.2. Hardness Results

Typically hardness distribution at various positions using Vickers (VHN) and Rockwell C (HRC) can be seen in Fig. 3. Vickers hardness contour on the link surface is in the range of 340 – 369 VHN. Referring to contours analysis, there is no specific pattern of VHN hardness on the sample surface. High VHN values can be found not only on the edge surface but also on the surface far from the edge.

Random VHN patterns are also found on the pin surface in Fig. 4 in the 412 – 463 VHN. The VHN pin hardness value is relatively higher than that in the link surface. Even in the as-received sample detected using the HRC test (Fig. 5.), the random patterns found on the HRC hardness value indicate the surface hardness of the failed sample, and the as-received sample does not experience a significant change in pattern.

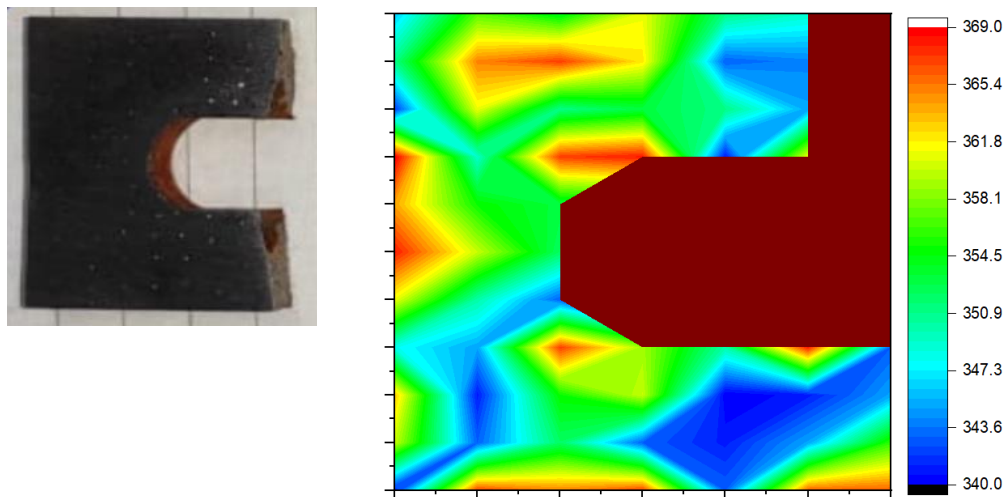


Fig. 3. Contour Vickers hardness test of surface fail link

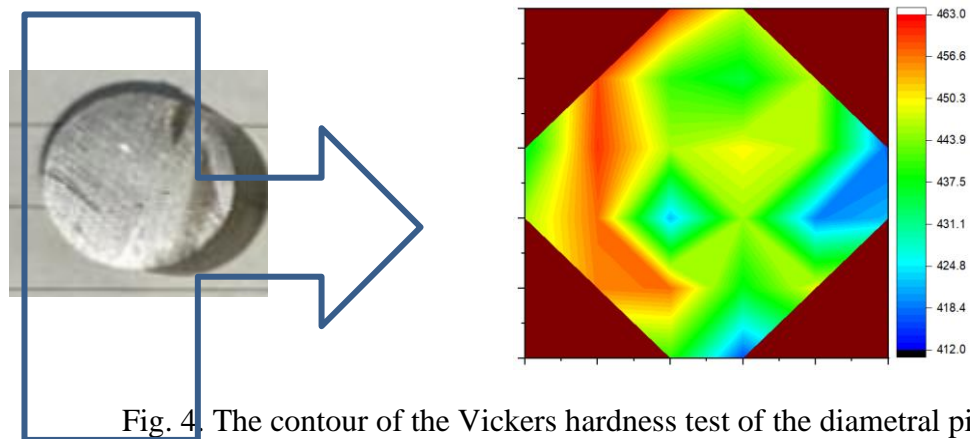


Fig. 4. The contour of the Vickers hardness test of the diametral pin

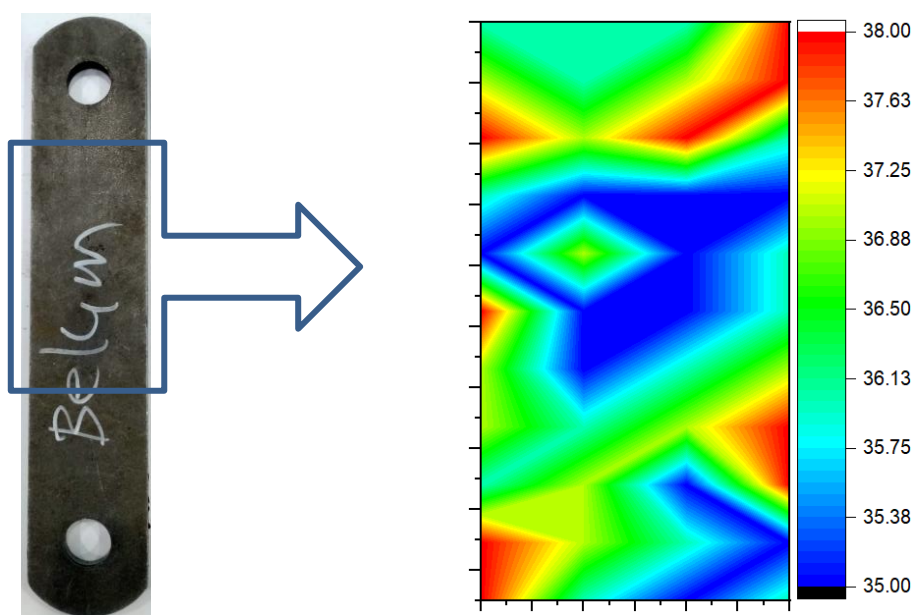
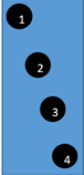


Fig. 5. Contour of HRC hardness test of surface as received link

In contrast, a steady pattern of HRC hardness can be found in the cross-sectional hardness of the link, where the hardness value has a standard deviation of 0.15 if the hardness is measured in the thickness direction, as can be seen at Table 2.

Table 2: Hardness Rockwell C (HRC) on thickness of as received link

Indenter Position	HRC	Cross Section of the Chain
1	36.5	
2	36.2	
3	36.3	
4	36.5	
Average	36.38	

4.3 Tensile Test

AISI 420 Martensitic stainless steels are widely used in steam generators, oil and gas exploration, overseas petroleum platforms, pressure valves, mixer blades, cutting tools, and surgical jigs. Owing to their excellent mechanical properties. In general, these steels are used in quenched and tempered conditions. Quenching heat treatment is carried out by cooling in oil or air followed by annealing at 980–1100 °C. Tempering is done at the interval of 200 and 700°C. Variation of the ultimate tensile strength (UTS) has a function of heat treatment temperature ranging from 900 to 1300 MPa. The tensile test was carried out using the standard JIZ Z 2201 test piece no.3. The results of this test, as presented in Table 3, show the ultimate stress value of 1060.89 N/mm² on average.

Table 3: The tensile test result of the as-received link

No.	Specimens	Area (mm ²)	Max. load (N)	Yield strength (N/mm ²)	Ultimate strength (N/mm ²)
1.	I	34.98	36695	941.87	1049.03
2.	II	34.98	37525	967.77	1072.76

4.4 Morphology Analysis

Fig. 6 shows the type of failed link. The fracture occurs in the pin-link joint hole in one or both end holes. The initial cracks were identified from the corrosion color, which was more concentrated than in other areas (Fig. 7). There are two main areas where crack initiation occurs; first, in the area that experiences higher residual stresses due to changes in dimensions that are not streamlined (notch root) as depicted in Fig. 7; second initial cracks occur in the middle of the pinhole. In both cases, in term of loading condition, it is believed that the cracks occurred due to the influence of the interference fit pin- links joint assembly and cyclic loading.

Many tests have demonstrated the beneficial effect of interference fit on metallic structures' fatigue resistance; recent results have shown beneficial effects. However, the material's yield stress and interference can produce local plastic deformations under normal load conditions. When an external load is applied, the pin and hole deform; slippage and contact loss can occur. Moreover, a multiaxial state of stress is produced.

Taking all these factors into account in prediction models is not simple. As explained previously, the beneficial effect of an interference fit is well known, but a quantitative prediction of this effect is difficult to make. Also, evaluating the stress state around an interference-fit pin is not easy unless simplifying hypotheses are introduced, such as elastic

behavior in all conditions and no separation between the sheet and pin when an external load is applied.

Some fatigue tests demonstrated that suppressing the transverse stress increases the fatigue life of faceted pins compared to round pins. However, crack nucleation could take place at different angles from the horizontal line as a function of the interference level. In open hole specimens, the notch root was the critical location.



Fig. 6. Typically fractured chain link

Macrostructure fractographic results are illustrated in Fig. 8; as shown, all specimens have negligible plastic deformation. However, there are some plastic deformation places and microvoids in specimens. A mixture of ductile and brittle mechanisms is visible in these specimens. The fracture appearance appears mainly as the cleavage and river pattern or brittle features mixing with a little ductile region. In addition, some voids are present in the fracture surface, probably formed at the matrix/carbide interfaces. Metallography observations also showed. Generally, the fracture was observed on vertex holes. The fracture surface consists of the initiation zone, the fibrous zone, the unstable zone, and the shear lips zone. Fig. 7. shows the profile of crack propagation across the initiation zone and fibrous zone.

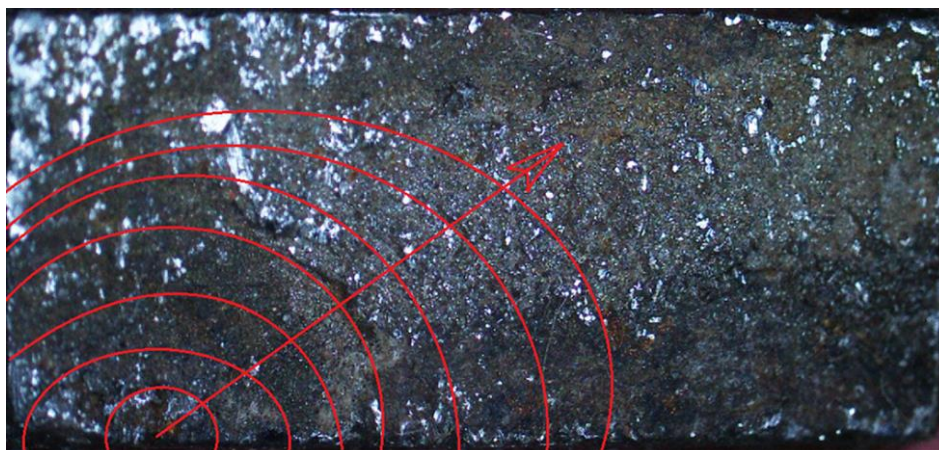


Fig. 7. Initial crack location and crack growth direction on the cross-section of the chain failed



Fig. 7 illustrates crack growth based on fractographic patterns and surface contours. Although the beach mark pattern as a general indication of fatigue failure is not visible, the relatively smooth surface contour with a circular pattern, as shown in Fig. 7, indicates the cracks propagate due to cyclical loading. A smooth fatigue fracture surface contour also indicates a very low load level compared to the material's tensile strength. Another evidence of a fatigue fracture mode can be seen in Fig. 8, where the link fails on both sides, but still, parts are connected. The fracture pattern clearly shows the link does not break apart suddenly due to excessive loads that exceed the tensile stress limit. However, fracture occurs slowly and gradually at low-stress levels.

The prior heat treatment done on the steel has a major influence on the final microstructure of AISI 420, which typically comprises martensite, un-dissolved and re-precipitate carbides, and retained austenite. The precipitation of carbides in the alloy during tempering is time-dependent, which involves precipitation of M_3C followed by M_7C_3 and then $M_{23}C_6$ type alloy carbides. Fig. 9. shows the fail link chain microstructure, which depicts large and small carbides inside the lath martensite associated with M_7C_3 and $M_{23}C_6$, respectively.

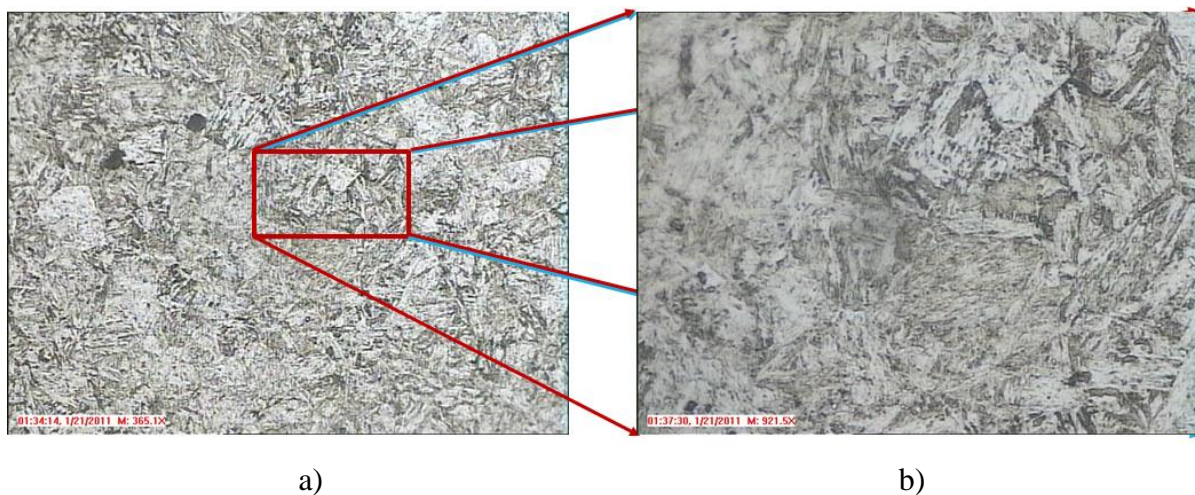


Fig. 8. Microstructure of failed link chain in the middle area



Fig. 9. Microstructure of fail sample, positioned near the edge of cross-section area

5. DISCUSSION

The material hardness, either as-received or failed link, did not show a significant difference in the hardness value and the pattern of hardness distribution. This is due to an inhomogeneous distribution of carbides in the microstructure. Then, the presence of retained austenite within lath martensite, which usually has a detrimental effect on hardness, is shown in Fig.s 10 and 11. As previously explained, inhomogeneous distribution was also detected on the as-received link of large and small carbides inside the lath martensite associated with M_7C_3 and $M_{23}C_6$. $M_{23}C_6$ carbide was found in colonies with the irregular shape of individual carbides. These carbides have very large sizes ranging from 15 to 20 microns.



Fig. 10. Microstructure of as-received surface link chain in the middle area

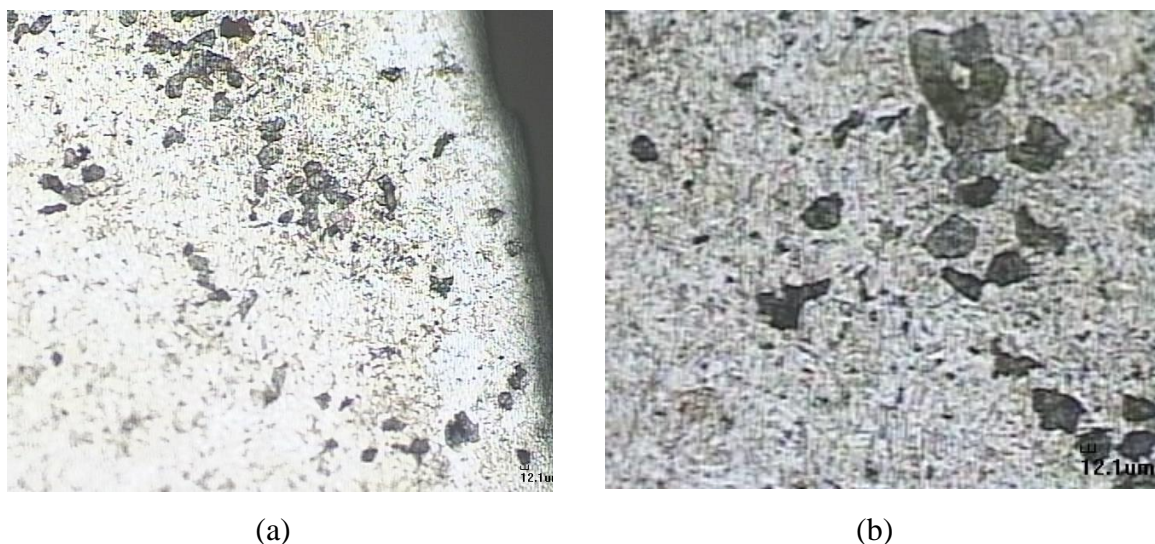


Fig. 11. Microstructure of as-received surface link chain: (a) near the edge, and (b). middle area

The tempered martensite microstructure of normalized-and-tempered ferritic/martensitic steels is more complicated than a solid solution, as shown (Fig. 11). During the normalization treatment, the steel is heated above the AC_3 temperature to transform the ferrite to a solid solution of austenite that transforms into body-centered tetragonal (BCT) martensite when it is air cooled.



During the tempering treatment below the AC1 temperature, the BCT martensite transforms to a BCC ferrite matrix with the accompanying precipitation of $M_{23}C_6$ (M is Cr rich with small amounts of Fe, Mn, Mo, W, etc.) and MX (M is Nb- and V-rich, depending on composition, with small amounts of Fe, Cr, Mo, etc., and X is C and N). Tempered martensite microstructure is a ferrite solid solution matrix containing a high density of the carbide precipitates primarily on subgrain boundaries (former martensite lath and packet boundaries) and prior-austenite grain boundaries [8].

Oxidation resistance is extremely important for high Cr steels in some applications. Chromium is the most effective alloying element to improve oxidation resistance. However, an increase of chromium content above 10% may result in the formation of δ -ferrite, which is a detrimental phase for creep strength and fracture toughness. As a result, at room temperature, the steel may become brittle and prone to cracking, especially under dynamic loading conditions [9].

The temperature at which a material transitions from ductile to brittle or brittle to ductile is called the 'Ductile to Brittle Transition Temperature' (DBTT) [10, 11]. The ductile to brittle transition temperature strongly depends on the metal's composition. Steel is the most commonly used metal that shows this behavior. Many cases have occurred throughout history where catastrophic failures have occurred due to brittle fractures [12, 13]. In terms of martensite stainless steel, many authors reported that the DBTT of martensite stainless steel is 0 - 50°C. The utilization of martensite stainless steel at this temperature should be considered due to the presence of DBTT temperature. Chain scrapper is equipment that is subjected to fatigue loading, especially under uniaxial loading. AISI 420 is categorized into martensite stainless steel and has the advantage of strength; on the other hand, it tends to brittle compare to other stainless-steel types.

6. CONCLUSION

Several investigations have been conducted on as-received and failed links so that some conclusions can be drawn:

1. Chain link failure occurs due to fatigue failure with very low-stress levels
2. Brittle fracture is found on the surface of the fractured specimen
3. Microstructures, XRD, and hardness properties showed no significant difference between as-received and failed links.
4. AISI 420 Chain link operates at ductile to brittle transition temperature (DBTT), where naturally, DBTT for AISI 420 steel is in the range 0 - 50°C.

Since the operating conditions of the chain are in a corrosive environment, experiencing dynamic loading and working temperatures between 23 and 60 °C, the selection of HSL materials such as AISI 4140 should be considered.

REFERENCES

- [1] F. Basim Ismail, E. Why Siew Kuan, and M. Shakir Nasif, "Development and implementation of bottom ash crushing system in Submerged Scrapper Conveyor (SSC) for Coal-fired Power Plant," *MATEC Web Conf.*, vol. 131, p. 03002, 2017. [Online]. Available: <https://doi.org/10.1051/mateconf/201713103002>.
- [2] A. Zbogor, F. Frandsen, P. A. Jensen, and P. Glarborg, "Shedding of ash deposits," *Progress in Energy and Combustion Science*, vol. 35, no. 1, pp. 31-56, 2009/02/01/ 2009, doi: <https://doi.org/10.1016/j.peccs.2008.07.001>.



- [3] L. Pattanayak, S. P. K. Ayyagari, and J. N. Sahu, "Optimization of sootblowing frequency to improve boiler performance and reduce combustion pollution," *Clean Technologies and Environmental Policy*, vol. 17, no. 7, pp. 1897-1906, 2015/10/01 2015, doi: 10.1007/s10098-015-0906-0.
- [4] L. Zhang and Z. Dong, "Analysis of Sootblowing Experiments and Research on Sootblowing Strategy for Coal-fired Utility Boiler," *IOP Conference Series: Earth and Environmental Science*, vol. 186, no. 5, p. 012033, 2018/09/01 2018, doi: 10.1088/1755-1315/186/5/012033.
- [5] S. Patel Sunny and R. K. M. Dr, "A Failure Analysis and Remaining Life assessment of Boiler Water Wall tube," *International Journal of Advanced Engineering Research and Science*, vol. 3, no. 7, 2016/7// 2016.
- [6] L. Deng, X. Tan, C. Tang, and D. Che, "A study on water-quenching waste heat recovery from molten slag of slag-tap boilers," *Applied Thermal Engineering*, vol. 108, pp. 538-545, 2016/09/05/ 2016, doi: <https://doi.org/10.1016/j.applthermaleng.2016.07.169>.
- [7] B. Beckhoff, h. B. Kanngießer, N. Langhoff, R. Wedell, and H. Wolff, *Handbook of Practical X-Ray Fluorescence Analysis*. 2006.
- [8] R. L. Klueh, "Analysis of swelling behaviour of ferritic/martensitic steels," *Philosophical Magazine*, vol. 98, no. 28, pp. 2618-2636, 2018/10/02 2018, doi: 10.1080/14786435.2018.1497307.
- [9] E. Bolli et al., "Cr Segregation and Impact Fracture in a Martensitic Stainless Steel," *Coatings*, vol. 10, no. 9, p. 843, 2020. [Online]. Available: <https://www.mdpi.com/2079-6412/10/9/843>.
- [10] W. D. Callister and D. G. Rethwisch, *Materials Science and Engineering: An Introduction, 9th Edition: Ninth Edition*. John Wiley and Sons, Incorporated, 2013.
- [11] G. Gunawan and A. Arifin, "Intergranular Corrosion and Ductile-Brittle Transition Behaviour In Martensitic Stainless Steel," *Indonesian Journal of Engineering and Science*, vol. 2, no. 3, pp. 029-039, 09/08 2021, doi: 10.51630/ijes.v2i3.23.
- [12] D. J. Benac, N. Cherolis, and D. Wood, "Managing Cold Temperature and Brittle Fracture Hazards in Pressure Vessels," *Journal of Failure Analysis and Prevention*, vol. 16, no. 1, pp. 55-66, 2016/02/01 2016, doi: 10.1007/s11668-015-0052-3.
- [13] J. F. Lancaster, "Failures of boilers and pressure vessels: Their causes and prevention," *International Journal of Pressure Vessels and Piping*, vol. 1, no. 2, pp. 155-170, 1973/04/01/ 1973, doi: [https://doi.org/10.1016/0308-0161\(73\)90020-3](https://doi.org/10.1016/0308-0161(73)90020-3).